Roller Drawing of Ultrahigh Molecular Weight Polyethylene

AKIRA KAITO, KAZUO NAKAYAMA, AND HISAAKI KANETSUNA,
Research Institute for Polymers and Textiles, 1-1-4, Yatabe-Higashi, Tsukuba, Ibaraki 305, Japan

Synopsis

The roller drawing of ultrahigh molecular weight polyethylene (UHMW-PE) sheets were carried out in the roller temperature T_r range of 100–140°C. In addition to the roller drawing in the solid state (T_r = 100°C), we attempted to crystallize the molten UHMW-PE sheet under the roller-drawing process (T_r = 100–140°C). The tensile and dynamic viscoelastic properties, the molecular orientation, and the microstructure of the roller-drawn UHMW-PE sheets were investigated. The mechanical properties of UHMW-PE sheets were much improved by crystallization during the roller drawing process at T_r = 140°C. The sheets roller-drawn at T_r = 135 and 140°C exhibited *c*-axis orientation to the draw direction and (100) alignment in the sheet plane. However, at T_r = 100°C the elastic motion of the amorphous chains induces the twinnings of lattice, which enhances the transition to the (110) alignment in the sheet plane. The dynamic storage modulus below γ-dispersion temperature showed good correlation with crystallinity and orientation functions, while taut tie molecules and thick crystallites play an important role in the storage modulus above γ-dipersion temperature.

INTRODUCTION

Ultrahigh molecular weight polyethylene (UHMW-PE) is known to posess some outstanding physical and mechanical properties such as high impact strength, abrasion resistance, self-lubrication, and resistance to the attack of chemicals.[1,2] As UHMW-PE contains a network superstructure formed by entanglements of long molecular chains,[3,4] UHMW-PE has very high melt viscosity, which limits its processibility by conventional forming techniques. Although solution-spun UHMW-PE fibers could be highly stretched to form high strength and high modulus fibers,[5] melt-crystallized UHMW-PE has poor extensibility compared with normal molecular weight high density polyethylene (HDPE) in the solid state.[4] Sakami et al.[6,7] reported that the UHMW-PE could be drawn to high draw ratio in the molten state. We also examined the uniaxial and biaxial drawing of UHMW-PE sheets in the molten state,[8,9] and found that the mechanical properties of UHMW-PE sheets were much improved by the uniaxial drawing in the molten state.[8] The improvement of mechanical properties can be explained by the alignment of entangled molecular chains in the draw direction during the melt drawing process. More recently Zachariades and Logan[10] reported melt flow crystallization of UHMW-PE under the combined effects of compression and rotation.

On the other hand, we recently examined the roller drawing of the HDPE sheet and showed the process useful for the production of high modulus

Journal of Applied Polymer Science, Vol. 30, 4591–4608 (1985)
 CCC 0021-8995/85/124591-18$04.00

polymer sheets.[11] In this method, the polymer sheets were uniaxially stretched to a high extension by drawing through a pair of heated rollers.

In this paper, we describe the application of the roller-drawing process to UHMW-PE. In addition to the roller drawing in the solid state, we attempt to crystallize molten UHMW-PE sheets under the roller-drawing process. The mechanical properties, the molecular orientation, and the microstructure of the roller-drawn UHMW-PE sheets are investigated.

EXPERIMENTAL

Sample Preparation

The sample used in this work was Hizex Million 240 M (Mitsui Petrochemical Co., with $\overline{M}_v$ = 1,900,000. The 240 M sheet 1.1 mm thick was cut into strips 30 mm wide, which were used for the experiment.

The apparatus used in this work was shown in the previous work.[11] A pair of heated rollers with a diameter of 50 mm were attached to the upper side of the crosshead of a tensile testing machine, Tensilon UTM-10T (Toyo Baldwin Co., Ltd.). The isotropic sheet was drawn through the rollers by lowering the crosshead of the tensile testing machine. The draw load was measured by a load cell mounted at the top of the tensile testing machine. The preheating temperature T_p and roller temperature T_r chosen in this work are summarized in the Table I along with the possible range of draw velocity v_d. The roller drawing of the molten sheets was carried out at T_r = 100–140°C after the sheet was melted at T_p = 150°C between preheating plates. Thereby the sheet was crystallized under the roller-drawing process.

Characterization

Tensile tests were carried out at 23 ± 1°C and a relative humidity of 50 ± 2% using a tensile testing machine, Tensilon UTM-III-100 (Toyo Baldwin Co.), with gauge length of 12.5 mm and a tensile rate of 4 mm/min. The dynamic viscoelastic properties were measured at 11 Hz with a dynamic viscoelastometer, Rheovibron DDV-II-EA (Toyo Baldwin Co.).

The wide angle X-ray diffraction (WAXD) intensity profile was measured using a scintillation counter. Ni-filtered Cu Kα radiation (40 kV,25 mA) produced by a Geiger Flex XGC-20 (Rigaku Denki Co.) was used. The crystallite sizes were calculated from the integrated line width using a Scherrer equation,[12] after the WAXD intensity profiles were corrected for Kα doublet and instrumental broadenings using reflections of silica.

TABLE I
Processing Temperature and Possible Range of Draw Velocity

	T_r (°C)	T_p (°C)	v_d (mm/min)
Roller- drawing in the solid state	100	100	≤500
Roller-drawing of the molten sheet	100	150	≤200
	135	150	≤200
	140	150	≤ 50

The 200 and 020 pole figures were obtained by employing both transmission and reflection techniques. The WAXD intensity was corrected for background and absorption.

The degree of orientation of the crystal *c*-axis was calculated from WAXD azimuthal scanning of 002 reflection, using Hermans orientation functions.[13]

Small angle X-ray scattering (SAXS) patterns were taken with a vacuum camera using Ni-filtered Cu Kα radiation (40 kV, 100 mA) produced by a Rota Flex RU-200 (Rigaku Denki Co.). In order to evaluate the long period, the SAXS intensity distribution was measured using a scintillation counter.

Birefringence was measured by the retardation method using a polarized microscope equipped with a Berek Compensator. The degree of orientation in the amorphous phase was estimated from birefringence using the equation proposed by Stein.[14] The values of 0.0585 and 0.12 were used for the intrinsic birefringences of the completely oriented crystalline and amorphous regions, respectively.[15]

The melting behavior of the samples was examined at a constant heating rate of 5°C/min with a Perkin-Elmer DSC-2 Differential Scanning Calorimeter calibrated with a melt transition of Indium (156.5°C).

Density was measured using an ethanol–water density gradient column at 25°C. The degree of crystallinity, the volume fraction of crystalline phase, was calculated assuming the densities of the crystalline and amorphous phases to be 0.999 and 0.8525 g/cm^3, respectively.[16,17]

RESULTS AND DISCUSSION

Appearance

The width of the UHMW-PE sheets decreased by the roller drawing. At T_r = 100°C (T_p = 100 and 150°C), the degree of width contraction increased from 15–17% to 23–26% with increasing draw velocity from 50 to 500 mm/min. At T_r=140 and 135°C (T_p = 150°C), the degree of width contraction was 0–22 % and decreased as the roller spacing was narrowed.

The UHMW-PE sheets became transparent by the roller drawing at T_r = 100 and 135°C, while the UHMW-PE sheets roller-drawn at T_r = 140°C (T_p = 150°C) were opaque.

Processing Condition and Deformation Behavior

The UHMW-PE sheets could be drawn in the draw velocity v_d range of 10–500 mm/min at T_r = T_p = 100°C. However, the upper limit of v_d decreased with the rise of T_r and T_p (Table I.). The roller drawing at T_r = T_p = 150°C was unsuccessful because of the occurance of stick-slip.

Drawing stress, draw ratio λ, and the ratio of sheet thickness after and before roller drawing, t/t_0, are plotted in Figure 1 as functions of the ratio of roller spacing to the original sheet thickness, t_r/t_0. Here, drawing stress is determed by the ratio of draw load to cross-sectional area of the original sheet, and draw ratio is defined by the ratio of length after and before roller drawing. The results at v_d = 50 mm/min are presented here.

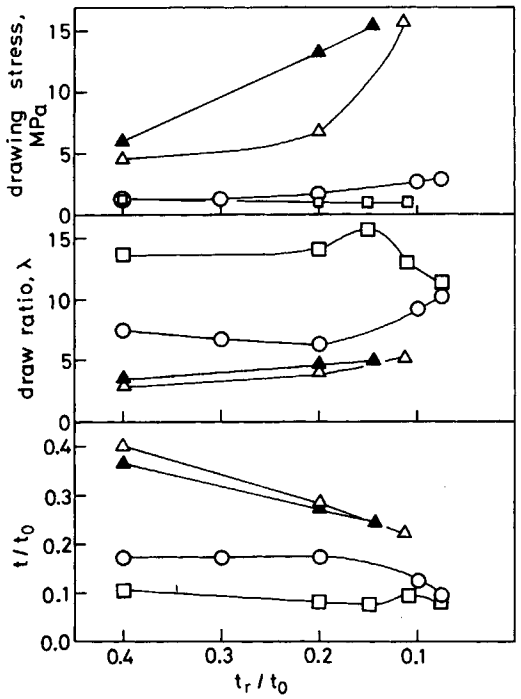

Fig. 1. Drawing stress, draw ratio (λ), and the ratio of sheet thickness after and before roller drawing (t/t_0) vs. the ratio of roller spacing to original sheet thickness (t_r/t_0); draw velocity, v_d = 50 mm/min. T_r, T_p (°C): (▲) 100, 100; (△) 100, 150; (○) 135, 150; (□) 140, 150.

The roller-drawing sheets were thicker than the roller spacing ($t/t_0 > t_r/t_0$) in the roller spacing range of $t_r/t_0 \leq 0.2$ at T_r = 100°C. The thickness of the UHMW-PE sheets recovered in part by the elastic motion of the amorphous region after they had passed through the rollers.

On the other hand, at T_r = 135 and 140°C (T_p = 150°C), the roller-drawn sheets were thinner than roller spacing ($t/t_0 < t_r/t_0$) in the range of $0.14 \leq t_r/t_0 < 0.4$. The sheets were not always in contact with roller surface throughout the deformation process, and stretched to a large extent after they had passed through the rollers.

At a given temperature condition, the draw ratio was changed with roller spacing and draw velocity. However, the possible range of draw ratio was much dependent on roller temperature; λ = 2.9–5.3 at T_r = 100°C. λ = 6.2–10.2 at T_r = 135°C, and λ = 11.3–15.9 at T_r = 140°C. The maximum draw ratio obtained by roller drawing at T_r = 100°C was higher than the value of λ = 3.33 achieved by hot rolling at same roller temperature.[18]

The drawing stress was much reduced by the rise of T_r from 100 to 140°C. At T_r = 100°C, the drawing stress increased with decreasing roller spacing.

Tensile Properties

The tensile properties of the roller-drawn UHMW-PE sheets are shown in Figure 2 as functions of draw ratio. The roller-drawn UHMW-PE were uniformly deformed without necking during tensile test. Although the ten-

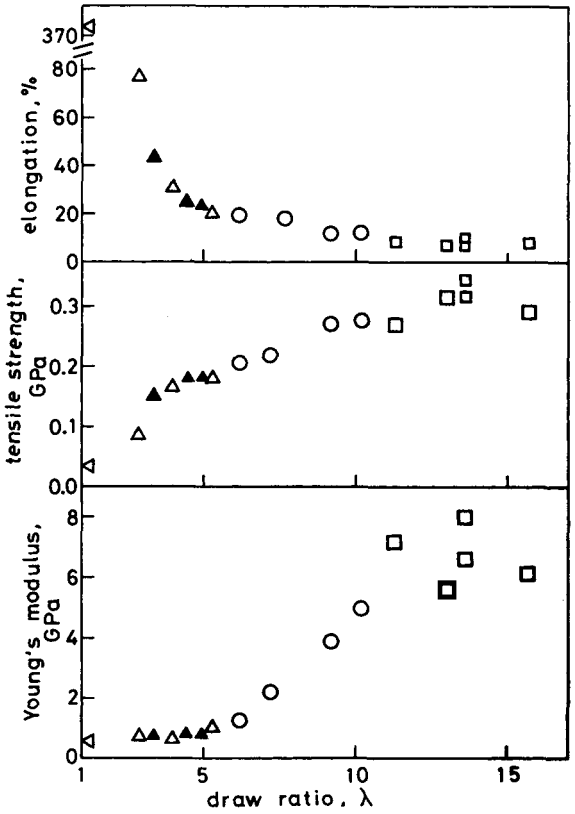

Fig. 2. Tensile properties vs. draw ratio (λ). T_r, T_p(°C): (▲) 100, 100; (△) 100, 150; (○) 135, 150; (□) 140, 150; (△) original 240 M sheet.

sile stength incrased with draw ratio at $\lambda \leq 5.3$ and $T_r = 100$°C, the Youngs's modulus was not much changed with draw ratio at $\lambda < 5.3$. The elongation at break rapidly decreased with draw ratio at lower draw ratio. At $6.2 \leq \lambda \leq 10.2$, $T_r = 135$°C, and $T_p = 150$°C, the Young's modulus and tensile stength increased with draw ratio. In particular, the increase in Young's modulus was remarkable in this draw ratio range. At $11 \leq \lambda \leq 16$, $T_r = 140$°C, and $T_p = 150$°C, the Young's modulus and the tensile strength did not systematically vary with draw ratio and lay in the range of 5.6–8.0 and 0.27–0.35 GPa, respectively.

Dynamic Viscoelastic Properties

Figure 3 shows the temperature dependence of dynamic viscoelatic properties of the roller-drawn UHMW-PE sheet. The tan δ peak located around −110°C (γ-dispersion peak) is associated with the initiation of micro-Brownian motion of amorphous chains. The tan δ peak of the roller-drawn sheet of $\lambda = 4.8$ and $T_r = T_p = 100$°C was higher than that of the original sheet, which was attributable to the increase in the degree of amorphous orientation by the roller-drawng at $T_r = T_p = 100$°C. The tan δ peak, however, became smaller with further increasing draw ratio and roller temperature.

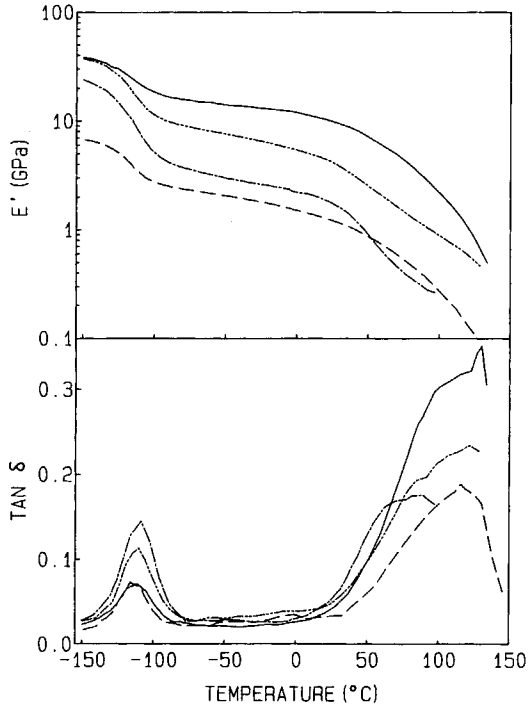

Fig. 3. Dynamic viscoelstic properties of roller-drawn UHMW-PE sheets: (- - -) original 240 M sheet; (- · · · · ·) $\lambda = 4.8$, $T_r = T_p = 100$°C; (- · · · · · · · · ·) $\lambda = 6.6$, $T_r = 135$°C, $T_p = 150$°C; (—) $\lambda = 14.0$, $T_r = 140$°C, $T_p = 150$°C.

The depression of the tan δ peak might be due to the increase of crystallinity and formation of taut tie molecules and thicker crystallites which would suppress the mobility of amorphous chains. The dynamic storage modulus (E') at -150°C was much increased by roller-drawing. However, the modulus of the roller-drawn sheet ($\lambda = 4.8$, $T_r = T_p = 100$°C) at room temperature was not much improved owing to the large fall of E' by the rise of temperature in the γ-dispersion region.

The tan δ peak observed around 80–130°C (α-dispersion peak) is associated with the molecular motion in the crystalline region. The tan δ peak of the roller-drawn sheet ($\lambda = 4.8$, $T_r = T_p = 100$°C) was shifted to the lower temperature side in comparison with the tan δ peak of the original sheet, suggesting that mobility of the crystalline region was enchanced by the roller drawing at $T_r = T_p = 100$°C. As the mobility of the crystalline region increased, the amorphous tie molecules which were registered to the crystalline region became relaxed, and the thermal shrinkage of the sheet proceeded. The dynamic storage modulus steeply decreased above room temperature and the degree of shrinkage exceeded 10 % at 100°C.

On the other hand, the sheets crystallized under roller drawing ($\lambda = 6.6$, $T_r = 135$°C and $\lambda = 14.0$, $T_r = 140$°C) showed the higher tan δ peak in the α-dispersion region than the original sheet. The increase of the tan δ peak might be attributed to the increase of crystal orientation, the degree of crystallinity, and crystalline perfection. The sheets roller-drawn at $T_r =$

135 and 140°C preserved higher dynamic storage moduli than the original sheet in the temperature range up to 130°C.

Pole Figure

The 200 and 020 pole figures measured for the roller-drawn sheet (λ = 3.4, $T_r = T_p$ = 100°C are shown in Figure 4. The principal axes of the sheet are labeled DD (draw direction), TD (traverse direction), and ND (normal direction). The contour lines were drawn in units of the intensity of a random sample. The pole figures suggested that the principal feature of crystal orientation was *c*-axis alignment to DD and (100) orientation in the sheet plane. The small maxima of 200 pole observed at 57° from ND to TD was considered to originate from (310) and (110) twinnings of latice.[19-21] The pole figures of the roller-drawn sheet (λ = 5.0, $T_r = T_p$ = 100°C) are shown in Figure 5. The 200 and 020 pole maxima were located at 60;° and at 30°. respectively, from ND to TD. The results are in coincidence with the alignment of (110) plane in the sheet plane. Hay and Keller[19] also reported the appearance of the (110) plane alignment in the heavily rolled low density polyethylene.

According to Hay and Keller,[19] the (100) plane aligns in the sheet plane during the rolling action and the (110) plane alignment arises only on removal of roller pressure. Elastic energy is stored in the amorphous region, while the roller pressure is acting. When the roller pressure is removed,

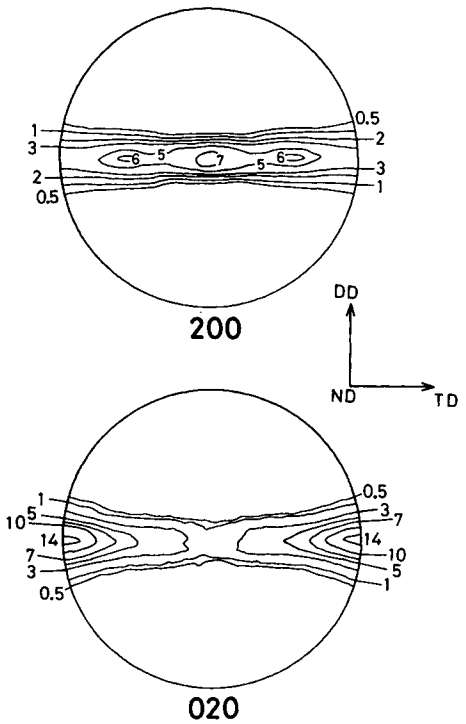

Fig. 4. 200 and 020 pole figures of the roller-drawn UHMW-PE sheet (λ = 3.4, $T_r = T_p$ = 100°C).

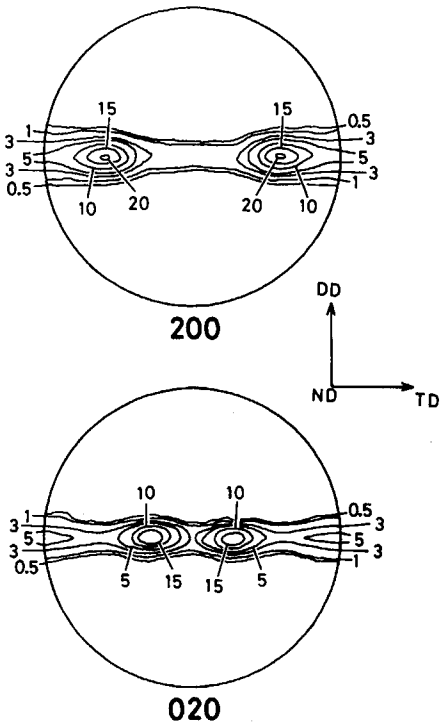

Fig. 5. 200 and 020 pole figures of the roller-drawn UHMW-PE sheet ($\lambda = 5.0$, $T_r = T_p = 100$°C).

the compressive force is generated along TD and becomes a driving force for the (310) and (110) twinnings. As roller spacing is narrowed, the amorphous region becomes highly strained during the roller pressure action, which generates a larger compressive force. Therefore, the (310) and (110) twinnings and transition to the (110) plane alignment are enchanced with increasing draw ratio.

The pole figures of the roller-drawn sheet ($\lambda = 5.3$, $T_r = 100$°C, $T_p = 150$°C) bore a strong resemblance to those of the sheet ($\lambda = 5.0$, $T_r = T_p = 100$°C) and are not shown here.

The pole figures of the roller-drawn sheet ($\lambda = 6.2$, $T_r = 135$°C, $T_p = 150$°C) are shown in Figure 6. The main feature was the (100) alignment in the sheet plane and high degree of orientation of the crystal c-axis to DD. The pole figures of the roller-drawn sheet ($\lambda = 10.2$, $T_r = 135$°C, $T_p = 150$°C) showed much similarity to those of the sheet ($\lambda = 6.2$, $T_r = 135$°C, $T_p = 150$°C), suggesting that draw ratio does not have much effect on crystal orientation at $T_r = 135$°C and $T_p = 150$°C. The large increase of Young's modulus in the range of $6.2 \leq \lambda \leq 10.2$ is considered to be due to the increase of number of tie molecules and crystalline bridges.

The pole figures of the roller-drawn sheet ($\lambda = 13.6$, $T_r = 140$°C, $T_p = 150$°C) are shown in Figure 7. Although the 200 and 020 pole maxima still remained at ND and TD, respectively, the 200 and 020 poles were distributed in the ND–TD line more symmetrically with respect to the axis of DD than those at lower processing temperatures.

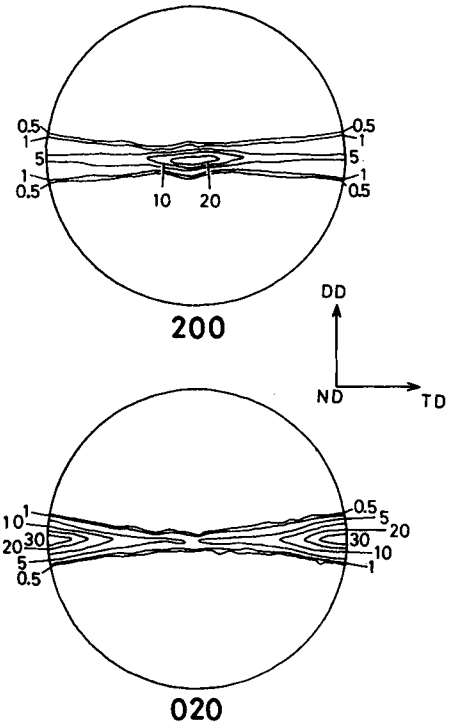

Fig. 6. 200 and 020 pole figures of the roller-drawn UHMW-PE sheet ($\lambda = 6.2$, $T_r = 135$°C, $T_p = 150$°C).

Degree of Orientation

The degree of orientation of the c-axis, f_c, and amorphous molecular chains, f_{am}, are shown in Figure 8. The results for roller-drawn HDPE sheet with $\bar{M}_w = 160{,}000$[11] are also included (◆) in Figure 8. Although f_c reached a constant value of 0.97–0.99 at $\lambda > 5$ irrespective of roller temperature, the value of f_{am} of UHMW-PE tends to decrease with the rise of roller temperature. Amorphous molecular chains in UHMW-PE were hard to orient to DD compared with those in normal molecular weight HDPE.

Small Angle X-ray Scattering

Figure 9 shows SAXS patterns of the roller drawn sheets with incident X-ray beam parallel to ND and TD (hereafter called ND-pattern and TD-pattern, respectively). A four-point diagram was observed the TD-pattern at $T_r = 100$ and 135°C, while no distinct SAXS diagram appeared in the ND-pattern. The crystalline and amorphous regions may be stacked alternately to form doubly oriented texture in the DD–ND plane. The angle ψ between the intensity maxima and the meridian corresponds to the angle between the direction of periodic layer stacking and DD. The long period L in the direction of periodic layer stacking can be obtained from the radial intensity distribution at ψ. The values of ψ, L, and the long period in the draw direction, $L/\cos\psi$, are summarized in Table II. The lamellar inclination angle ψ increased with increasing draw ratio at $T_r = 100$°C. The

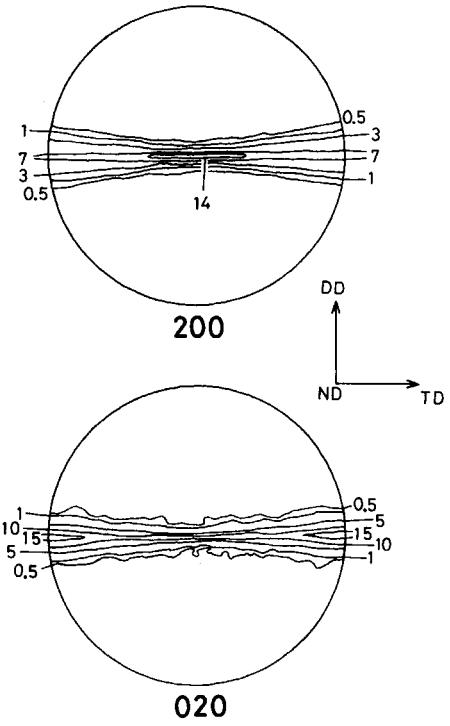

Fig. 7. 200 and 020 pole figures of the roller-drawn UHMW-PE sheet ($\lambda = 13.6$, $T_r = 140$°C, $T_p = 150$°C).

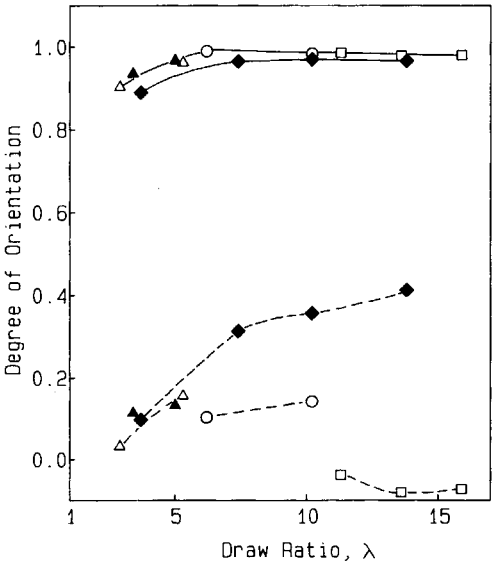

Fig. 8. Degree of orientation in crystalline (—) and amorphous (- - -) regions vs. draw ratio (λ). T_r, T_p (°C): (▲) 100, 100; (△) 100, 150; (○) 135, 150; (□) 140, 150; (◆) HDPE sheet, 100, 100.

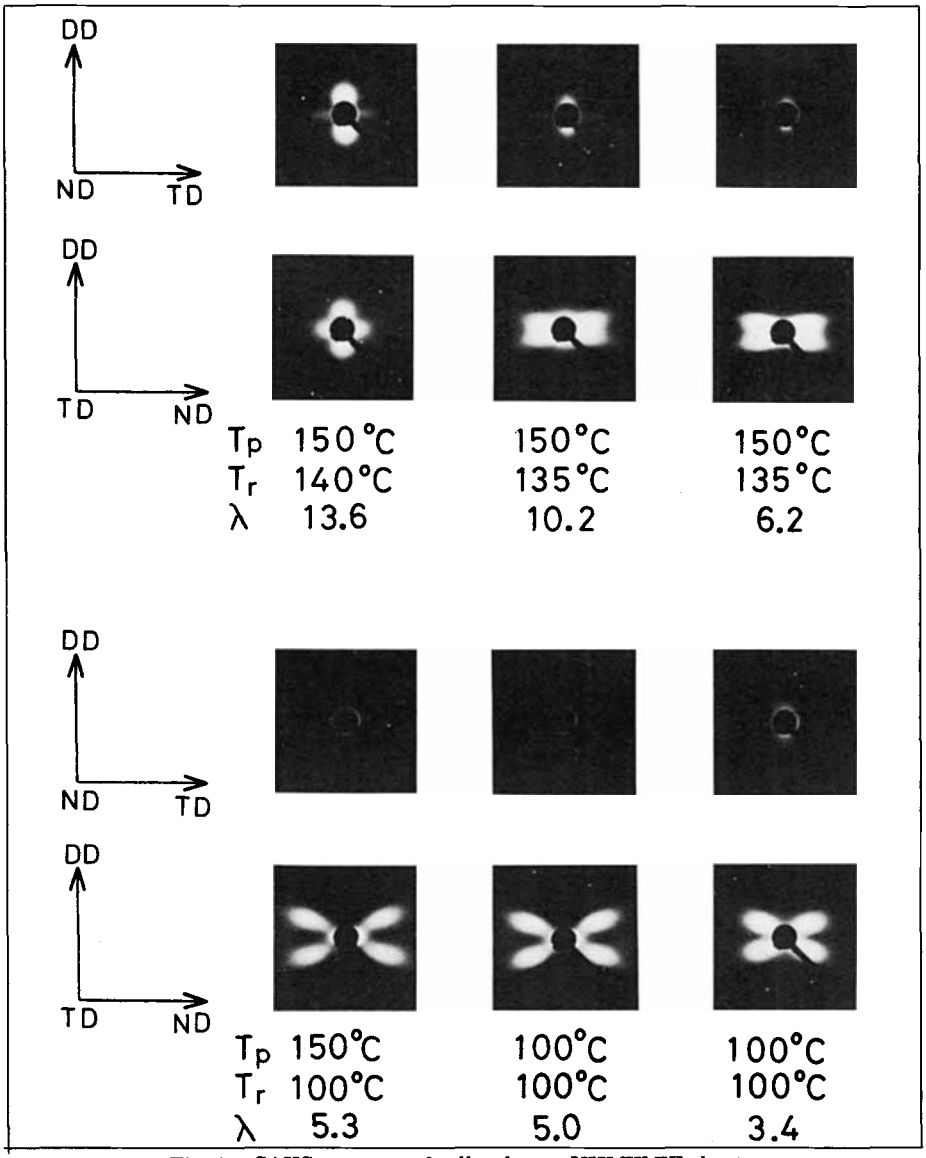

Fig. 9. SAXS patterns of roller-drawn UHMW-PE sheets.

highly inclined texture ($\psi = 71\text{-}72°$) was formed in the sheet roller-drawn at $T_r = 135°C$ and $T_p = 150°C$.

On the other hand, a two-point diagram was exhibited on the meridian in the ND- and TD-patterns of the roller-drawn sheet ($\lambda = 13.6$, $T_r = 140°C$, $T_p = 150°C$). The crystalline and amorphous regions are considered to be stacked alternately along DD, at periodic intervals of 52 nm (Table II). In the TD-pattern, the additional SAXS was observed on the equator. Although its origin is not clearly known, the long periodic structure would be present along ND.

TABLE II
SAXS Results of the Roller-Drawn UHMW-PE sheets

T_r (°C)	T_p (°C)	λ	Ψ (°)	L (nm)	$L/\cos\psi$ (nm)
100	100	3.4	62	28.8	61
100	100	5.0	64.5	19.6	46
100	150	2.9	42	30.5	41
100	150	5.3	65	18.1	43
135	150	6.2	71	a	
135	150	9.2	72	a	
135	150	10.2	72	a	
140	150	11.3[b]	73	a	
140	150	13.6	0	52	52
140	150	14.0	0	52	52

[a] The four-point SAXS diagram was not resolved from central diffuse scattering.
[b] Prepared at narrow roller spacing ($t_r/t_0 = 0.07$).

Crystallite Size and Crystallinity

The crystallite sizes in the direction normal to the (200), (020), and (002) planes, D_{200}, D_{020}, and D_{002}, and a volume fraction of crystalline phase, X_v, are shown in Table III. The value of D_{200} decreased by roller drawing at $T_r = 100$°C, suggesting that the cleavage of crystallites occured along the (100) plane by intracrystallite slip at the initial stage of the roller-drawing process. The crystallite sizes and the degree of crystallinity were not much dependent on draw ratio, but considerably increased with the rise of roller temperature.

Melting Behavior

The DSC curves of the UHMW-PE sheets are shown in Figure 10. The melting peak shifted to the higher temperature region in the roller-drawn sheets (λ = 5.0, $T_r = T_p = 100$°C, and λ = 6.2, $T_r = 135$°C, $T_p = 150$°C)

TABLE III
Crystallite Sizes (D_{200}, D_{020}, and D_{002}) and Volume Fraction of Crystalline Phase (X_v) of the Roller-Drawn UHMW-PE Sheets

T_r (°C)	T_p (°C)	λ	D_{200} (nm)	D_{020} (nm)	D_{002} (nm)	X_v (%)
Original sheet		1	17.1			50.0
100	100	3.4	11.6	12.8	19.4	48.5
100	100	5.0	11.4	11.7	18.9	49.3
100	150	2.9	12.3	13.5	17.3	50.7
100	150	5.3	11.0	11.0	17.1	50.7
135	150	6.2	16.1	15.4	23.7	54.7
135	150	9.2	15.7	14.1	23.7	68.4
135	150	10.2	14.8	14.4	24.3	68.9
140	150	11.3[a]	17.6	14.9	26.4	71.7
140	150	13.6	17.9	15.1	24.9	67.5
140	150	15.9	19.2	15.0	25.1	67.8

[a] Prepared at narrow roller spacing ($t_r/t_0 = 0.07$).

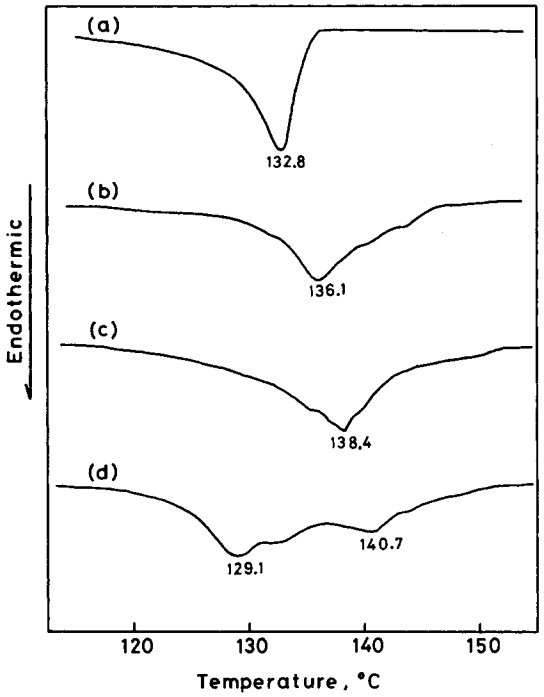

Fig. 10. DSC curves for UHMW-PE sheets: (a) original sheet; (b) $\lambda = 5.0$, $T_r = 100°C$, $T_p = 100°C$; (c) $\lambda = 6.2$, $T_r = 135°C$, $T_p = 150°C$; (d) $\lambda = 13.6$, $T_r = 140°C$, $T_p = 150°C$.

[Figs. 10(b) and 10(c)]. The molecular chains would come in an extended form, and the amorphous region would be strained by the roller-drawing at these temperatures.

The sheet ($\lambda = 13.6$, $T_r = 140°C$, $T_p = 150°C$) exhibited two melting peaks on the DSC curve. The one at 140.7°C might be due to the crystallites crystallized at the initial stage of the roller-drawing process. Another at 129.1°C would be attributable to the crystallites formed under nonisothermal tensile flow in the post-roller zone.

Comparison with the Roller-Drawing of HDPE

The HDPE sheet with $\overline{M}_w = 61{,}000$ could be stretched up to $\lambda = 25$ by the roller drawing at $T_r = T_p = 100°C$.[11] However, the maximum draw ratio attained for UHMW-PE was as low as 5.0 under the same temperature condition. The reason for the difference is that extensibility is restricted by the entanglement of long molecular chains in the UHMW-PE sheet.

As the chain entanglement form a network superstructure,[3,4] UHMW-PE loses fluidity and shows rubberlike elasticity in the melt. The entangled molecular chains become aligned in the draw direction by stretching the molten UHMW-PE sheet. Therefore, the roller drawing of molten sheet is effective for UHMW-PE.

As the chain entanglements are excluded from the crystalline region, UHMW-PE contains larger amount of entangled noncrystalline chains than normal molecular weight HDPE. In the roller drawing of UHMW-PE at

T_r = 100°C, the elastic motion of the amorphous region would make considerable contribution to the deformation process, which induces the thickness recovery on the removal of roller pressure. In addition, the elastic energy stored in the amorphous region of UHMW-PE during the roller pressure action generates sufficient compressive forces to induce the twinnings of lattice. In the heavily roller-drawn UHMW-PE sheet (λ = 5.0, T_r = T_p = 100°C), the texture was completely transformed to the (110) plane alignment. On the other hand, in the roller drawing of normal molecular weight HDPE,[11] the elastic motion of the amorphous region is not enough to induce thickness recovery and the (110) plane alignment.

Effect of Processing Temperature

The microstructure of the roller-drawn UHMW-PE sheets was much dependent on processing temperatures, T_r and T_p. Effects of processing temperatures on the roller drawing process of UHWM-PE are shown in Figure 11. The characteristics in microstructure in each case is summarized in Table IV.

In case (a), the UHMW-PE sheet is deformed in the solid state accompanied by partial thickness recovery.

In case (b), the UHMW-PE sheet melted in the preheating zone is crystallized soon after the sheet has come in contact with roller surface. Then, the sheet is deformed in the solid state between rollers, similarly to the case (a). The roller-drawn sheets show much similarity to those in case (a) in maximum draw ratio, crystal orientation, and microstructure.

In case (c), the molten UHMW-PE sheet is crystallized under roller pressure and tensile stress between rollers. The roller drawing at T_r = 135°C corresponds to this case. At narrow roller spacing (t_r/t_0 < 0.1), the roller

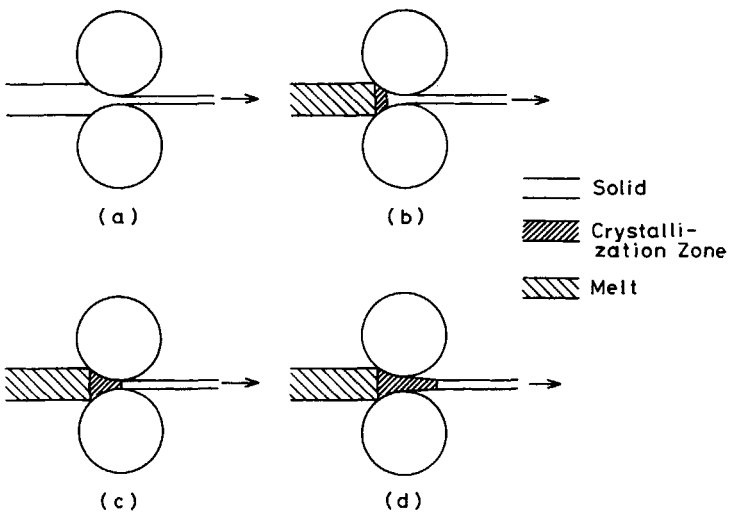

Fig. 11. Effect of processing temperature on the roller-drawing process: (a) T_r = 100°C, T_p = 100°C; (b) T_r = 100°C, T_p = 150°C; (c) T_r = 135°C, T_p = 150°C and T_r = 140°C, T_p = 150°C, t_r/t_0) < 0.1; (d) T_r = 140°C, T_p = 150°C, $t_r/t_0 \geq 0.1$.

TABLE IV
Summary of Crystal Orientation and Microstructure of the Roller-Drawn UHMW-PE Sheets

Case	Crystal orientation[a]	SAXS pattern
a	(100)[001] + (110)[001] (λ = 3.4) (110)[001] (λ = 5.0)	Four-point diagram (ψ = 62–65°)
b	(100)[001] (λ = 2.9) (110)[001] (λ = 5.3)	Four-point diagram (ψ = 42–65°)
c	(100)[001]	Four-point diagram (ψ = 71–73°)
d	(100)[001] (the a - and b-axes are more symmetrically distributed in the ND–TD plane than in other cases.)	Two-point diagram(ψ = 0°)

[a] $(abc)[xyz]$ represents that the (abc) plane is oriented in the sheet plane and the $[xyz]$ axis is parallel to the draw direction.

pressure enhances crystalliztion between rollers even at T_r = 140°C (above melting temperature of UHMW-PE under atmospheric pressure). The sheet roller-drawn at T_r = 140°C and t_r/t_O = 0.07 also belongs to this case.

In case (d) ($t_r/t_O > 0.1$, T_r = 140°C), the crystallization of UHMW-PE takes place not only between rollers, but also under tensile flow in the post roller zone. The roller-drawn sheets show a two-point SAXS diagram on the meridian similarly to the melt drawn UHMW-PE sheets.[8]

Relationship between Elastic Modulus and Structure

On the basis of two-phase model, Seferis and Samuels[22] proposed a compliance equation which predicts mechanical properties of a uniaxially oriented polymers from crystallinity and orientation functions. If uniform distribution of stress is assumed (Ruess model), the complience array of bulk materials is expressed as

$$S_{ij} = X_v\langle S_{ij}\rangle_c + (1 - X_v)\langle S_{ij}\rangle_{am} \tag{1}$$

where $\langle S_{ij}\rangle_c$ and $\langle S_{ij}\rangle_{am}$ are the compliances of the crystalline and amorphous phases, respectively. By assuming that the axial tensile compliance of each phase is much smaller than the traverse tensile compliance, and that the axial shear compliance is eaual to the traverse tensile compliance,eq. (1) leads to a two-parameter form[22]

$$1/E = A_c X_v (1 - f_c) + A_{am} (1 - X_v)(1 - f_{am}) \tag{2}$$

where A_c and A_{am} can be related to traverse Young's moduli of crystalline and amophous phases, $E_c^{\perp}$ and $E_{am}^{\perp}$ respectively:

$$A_c = 2/3E_c^{\perp} \tag{3}$$

$$A_{am} = 2/3E_{am}^{\perp} \tag{4}$$

By dividing eq. (2) by $(1 - X_v)(1 - f_{am})$, one obtains

$$1/E(1 - X_v)(1 - f_{am}) = A_c X_v (1 - f_c)/(1 - X_v)(1 - f_{am}) + A_{am} \quad (5)$$

Figure 12 shows plots of $1/E(1 - X_v)(1 - f_{am})$ vs. $X_v(1 - f_c)/(1 - X_v)(1 - f_{am})$, in which the results for the roller-drawn HDPE sheets[11] are included. Figures 12(a) and 12(b) were obtained by using the values of dynamic storage modulus at −145 and at −50°C, respectively.

The dynamic storage modulus at −145°C (below γ-dispersion temperature) had a close relation with crystallinity and orientation functions and was in conformity with the Seferis model[22] [Fig. 12(a)]. On the other hand, the dynamic storage modulus at −50°C (above γ-dispersion temperature) showed poor correlation with crystallinity and orientation functions except for $\lambda < 6$. The deviation from Seferis model became remarkable as draw ratio increased [Fig. 12(b)].

According to the deformation mechanism proposed by Peterln,[23,24] amorphous taut tie molecules are formed in the intercrystallite and interfibrilar regions. The tie molecules increase in number and tautness with increasing draw ratio. The roller-drawn sheet ($\lambda = 13.6$, $T_r = 140$°C, $T_p = 150$°C) showed a melting peak at temperature as high as 140.7°C, suggesting the presence of thick crystallites. As the mobility of amorphous molecular

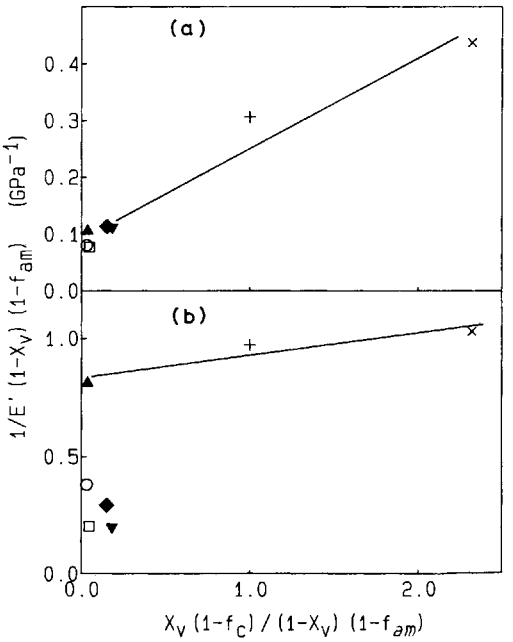

Fig. 12. $1/E'(1 - X_v)(1 - f_{am})$ vs. $X_v(1 - f_c)/(1 - X_v)(1 - f_{am})$: (a) the value of E' at −145°C is used; (b) the value of E' at −50°C is used; (+) original UHMW-PE sheet; (▲) UHMW-PE, $\lambda = 4.8$, $T_r = T_p = 100$°C; (○) UHMW-PE, $\lambda = 6.6$, $T_r = 135$°C, $T_p = 150$°C; (□) UHMW-PE, $\lambda = 14.0$, $T_r = 140$°C, $T_p = 150$°C; (×) original HDPE sheet; (◆) HDPE, $\lambda = 6.6$, $T_r = T_p = 100$°C; (▼) HDPE, $\lambda = 13.5$, $T_r = T_p = 100$°C.

chains increases by the rise of temperature above the γ-dispersion region, stress is selectively distributed to the tie molecules and thick crystallites which interconnect the crystalline region. Above the γ-dispersion region, mechanical properties are no longer explained by the Seferis model and might be sensitive to the fraction of taut tie molecules and thick crystallites.

CONCLUSION

The roller-drawing technique was found to be applicable to the deformation of UHMW-PE sheets in the roller temperature range of 100–140°C. The Young's modulus and tensile strength were much improved by drawing the molten UHMW-PE sheet through the rollers at T_r = 135–140°C.

At T_r = 100°C, the elastic motion of amorphous molecular chains induces the twinnings of lattice, which enhances the transition to the (110)[001] texture from the (100)[001]texture. The lattice twinnings were not observed in the sheet roller-drawn at T_r = 135 and 140°C. The sheets roller-drawn at T_r = 140°C and $t_r/t_0 > 0.1$ showed a two-point SAXS diagram, suggesting that the crystalline and amorphous regions are stacked alternately along DD. On the other hand, the sheets roller-drawn at T_r = 100 and 135°C have the periodic structure in which the direction of the periodic layer stacking is inclined in the ND–TD plane.

The Seferis model, a two-phase model which predicts mechanical properties of oriented polymers from crystallinity and orientation functions, explains well the dynamic storage modulus below γ-dispersion temperature, but fails to describe the mechanical properties above γ-dispersion temperature. The stiffening by the increase of amorphous taut tie molecules and thick crystallites becomes a dominant factor in the mechanical properties above γ-dispersion temperature.

References

1. M. Takiura and M. Ishida, *Plastics,* **25(4)**, 77 (1974).
2. T. Shiraki, *Plastics,* **28(5)**, 57 (1977).
3. J. Steidel and Z. Pelzbauer *J. Polym. Sci., C,* **38,** 345 (1972).
4. G. Capaccio, T. A. Crompton, and I. M. Ward, *Polymer,* **17,** 644 (1976).
5. P. Smith and P. J. Lemstra, *J. Mater.Sci.,* **15,** 505 (1980).
6. H. Sakami, S. Iida, and K. Sasaki, *Kobunshi Ronbunshu,* **34,** 653 (1977).
7. H. Sakami and T. Izushi, *Kobunshi Ronbunshu,* **26,** 575 (1979).
8. A. Kaito, K. Nakayama, and H. Kanetsuna, *Polym. J.,* **14,** 757 (1982).
9. A. Kaito, K. Nakayama, and H. Kanetsuna, *J. Appl. Polym. Sci.,* **29,** 2347 (1984).
10. A. E. Zachariades and J. A. Logan, *J. Appl. Polym. Sci.,* **28,** 1837 (1983).
11. A. Kaito, K. Nakayama, and H. Kanetsuna, *J. Appl. Polym. Sci.,* **30,** 1241 (1985).
12. P. Scherrer, *Gött. Nachr.,* **2,** 98 (1918).
13. P. H. Hermans, *Physics and Chemistry of Cellulose Fibers,* Elsevier, Amsterdams, 1949.
14. R. S. Stein, *J. Polym. Sci.,* **31,** 327 (1958).
15. A. R. Wedgewood and J. C. Seferis, *Polym. Eng. Sci.,* **24,** 328 (1984).
16. P. R. Swan, *J. Polym. Sci.,* **56,** 403 (1962).
17. M. G. Gubler and A. G. Kovacs, *J. Polym. Sci.,* **34,** 551 (1959).
18. A. Kaito, K. Nakayama, and H. Kanetsuna, *J. Appl. Polym. Sci.,* **28,** 1207 (1983).
19. I. L. Hay and A. Keller, *J. Mater. Sci.,* **1,** 41, (1966).

20. D. Lewis, E. J. Wheeler, W. F. Wheeler, W. F. Maddams, and J. E. Preedy, *J. Polym. Sci., A-2,* **10**, 369 (1972).
21. O. Yoda and I. Kuriyama, *J. Polym. Sci., Poly. Phys. Ed.,* **15**, 773 (1977).
22. J. C. Seferis and R. J. Samuels, *Polym. Eng. Sci.,* **19**, 975 (1979).
23. A. Peterlin, *J. Polym. Sci., A-2,* **7**, 1151 (1969).
24. A. Peterlin, *J. Mater. Sci.,* **6**, 490 (1971).

Received December 5, 1984
Accepted March 11, 1985